European Journal of Pharmaceutical Sciences 189 (2023) 106550

Contents lists available at ScienceDirect

European Journal of Pharmaceutical Sciences

journal homepage: www.elsevier.com/locate/ejps

Biophysical and docking study on the interaction of anticancer drugs encorafenib and binimetinib with human serum albumin

Gabriele Cavalieri [a], Giulia Cilurzo [a], Lorenzo Pettorosso [a], Andrea Mansueto [a], Erik Laurini [a,*], Sabrina Pricl [a,b]

[a] Molecular Biology and Nanotechnology Laboratory (MolBNL@UniTS), DEA, University of Trieste, Piazzale Europa 1, 34127 Trieste, Italy
[b] Department of General Biophysics, Faculty of Biology and Environmental Protection, University of Lodz, ul. Pomorska 141/143, 90-236 Łódź, Poland

ARTICLE INFO

Keywords:
Encorafenib
Binimetinib
Human serum albumin
Fluorescence spectroscopy
Isothermal titration calorimetry
Molecular simulations

ABSTRACT

The utilization of BRAF and MEK inhibitors in combination therapy has demonstrated superior outcomes in the treatment of melanoma as compared to monotherapy. In the present scenario, the combination therapy of Encorafenib (ENC), a BRAF inhibitor, and Binimetinib (BINI), a MEK inhibitor, has been identified as one of the most efficacious treatment modalities for this malignancy. Investigations of protein binding, particularly with human serum albumin (HSA), are essential to understand drug performance and enhance therapeutic outcomes. The investigation of the interplay between small molecule drugs and HSA is of paramount importance, given that such interactions can exert a substantial influence on the pharmacokinetics of these therapeutic agents. The present study aims to bridge these lacunae by implementing a comprehensive approach that integrates fluorescence spectroscopy (FS), isothermal titration calorimetry (ITC), far-ultraviolet circular dichroism (far-UV CD), and molecular simulations. Through analysis of the fluorescence quenching of HSA at three distinct temperatures, it was ascertained that the association constants for the complexes formed between drugs and HSA were of the magnitude of 10^4 M^{-1}. This suggests that the interactions between the compounds and albumin were moderate and comparable. Simultaneously, the investigation of fluorescence indicated a contrasting binding mechanism for the two inhibitors: ENC predominantly binds to HSA through enthalpic interaction, while BINI/HSA is stabilized by entropic contributions. The data obtained was confirmed through experimental procedures conducted using the ITC method. The results of ligand-competitive displacement experiments indicate that ENC and BINI can bind to HSA within subdomain IIA, specifically Sudlow site I. However, far-UV CD studies show that there are no notable alterations in the structure of HSA upon binding with either of the two inhibitors. Ultimately, the results were supported by computational molecular analysis, which identified the key interactions that contribute to the stabilization of the two ligand/HSA complexes.

1. Introduction

According to data from the SEER database, the National Cancer Institute (NCI) and the American Cancer Society (ACS), for the year 2023 approximately 97,610 newly diagnosed cases of melanoma and 7990 associated fatalities are predicted within the United States. Melanoma of the skin is a relatively prevalent form of cancer when compared to other types of cancer. It ranks as the fifth most common cancer, accounting for 5.2% of all newly diagnosed cancer cases in the United States (SEER, 2023). In Europe, by 2020 the estimated number of new melanoma cases in EU-27 nations by the European Cancer Information System (ECIS) was 106,369 (with 16,488 related deaths); however, the current predicted incidence of this pathology up to 2040 forecasts an increase of 13.7% and 29.4% in new cases and mortality, respectively, positioning it as the sixth most prevalent form of cancer based on frequency of occurrence (ECIS, 2023).

Cutaneous melanoma (CM) is the deadliest of all skin malignancies, with a median age at the time of diagnosis of 59 years. The prognosis of melanoma is largely determined by the stage at which the disease is discovered (Miller et al., 2020). As per the American Joint Committee on Cancer (AJCC) TNM system, melanoma is categorized into stages I-IV, which delineate the extent of cancer in the organism, based on three parameters: the tumour (T) (comprising thickness and ulceration), the dissemination to adjacent lymph nodes (N), and the metastasis to remote

* Corresponding author.
E-mail address: erik.laurini@dia.units.it (E. Laurini).

https://doi.org/10.1016/j.ejps.2023.106550
Received 26 June 2023; Received in revised form 21 July 2023; Accepted 28 July 2023
Available online 30 July 2023

locations (M)(ACS, 2023). The observed survival rate for individuals initially diagnosed with stage I-II disease over a period of 5 years (2011–2017) is 99.4%, while the rate drops to 68.0% for stage III and 29.8% for stage IV. Merely 4% of diagnoses are established in stage IV, whereas 83% of diagnoses are detected in stages I-II. As per the SEER database, the 5-year overall survival rate for melanoma is 93.3% (Saginala et al., 2021).

The BRAF gene produces three Raf serine/threonine kinase (STK) isoforms (A-Raf, B-Raf, and C-Raf), all of which are involved in the mitogen-activated protein kinase (MAPK) signalling cascade regulating cell growth, differentiation, and survival (Dhillon et al., 2007). About 2 decades ago, melanomas were found to harbour several driver mutations in various members of the MAPK pathways, variations in BRAF being the most common event (approximately 50%). Amongst the most frequently observed BRAF mutations, the missense substitution V600E appears in 74%−90% of cases, followed by V600K (15%−25% of V600 mutations), V600R, and V600D, although other rarer mutations (*i.e.*, V600A, V600M, and V600G) have also been reported (Dankner et al., 2018).

The therapeutic landscape for the treatment of metastatic melanoma has undergone a significant transformation in recent times, consequent to the approval of targeted therapy drugs for clinical use by the American Food and Drug Administration (FDA) and European Medicines Agency (EMA), and the relevant clinical trials have indeed established that the inhibition of BRAF function results in an effective suppression of melanoma cell proliferation. This paved the way to the approval in 2013 of a class on BRAF inhibitors (BRAFi) like Vemurafenib (Zelboraf, Roche) and Dabrafenib (Tafinlar, GlaxoSmithKline) (Rheault et al., 2013).

It is noteworthy that the administration of BRAF inhibitors elicits distinctive adverse reactions, including photosensitivity and the swift onset of cutaneous squamous cell carcinoma (cuSCC), which manifests in roughly 14–26% of BRAFi-treated patients, typically during the initial 2–3 months of therapy. The formation of these cutaneous neoplasms is a result of a paradoxical activation of the MAPK pathway in keratinocytes, which is triggered by the pre-existing RAS mutations upstream of the signalling cascade. However, this process can be inhibited by the administration of a MEK inhibitor (MEKi) (Larkin et al., 2014). Therefore, co-administration of BRAF and MEK inhibitors was predicted to mitigate this adverse event, and, in fact, this combinatorial therapeutic approach not only yielded a statistically significant improvement in progression-free survival (PFS) and overall survival (OS) relative to BRAFi monotherapy, but also elicited a reduction in cuSCC incidence.

Today, an important combination of BRAFis and MEKis is represented by Encorafenib (ENC) (Braftovi) + Binimetinib (BINI) (Mektovi), two orally bioavailable drugs developed by Array BioPharma. They both obtained their first global approval in the USA in June 2018 for the treatment of patients with metastatic or incurable melanoma who carry the BRAFV600E or -V600K mutation based on the result of COLUMBUS trial. In this trial, 577 patients with advanced melanoma expressing the BRAFV600E/V mutation were randomly assigned to one of three treatment groups: ENC + BINI, ENC, or Vemurafenib monotherapy. The combination group exhibited superior outcomes, with a median OS of 33.6 months, compared to 23.5 months and 16.9 months for the other groups, respectively. The clinical development of the ENC + BINI combination therapy for the treatment of metastatic colorectal cancer is also currently ongoing in phase III (Shirley, 2018; Teixido et al., 2021).

In general, the *in vivo* activity of a drug is considered to be governed by its pharmacokinetic (PK) and pharmacodynamic (PD) properties, which can be influenced by factors such as absorption, distribution, metabolism, and excretion (ADME). Numerous physiological processes exhibit a direct correlation with the ability of a drug to bind to plasma proteins (PPs). This, in turn, impacts the drug's ADME properties and ultimately determines the relevant clinical outcomes. Any pharmacological agent that exhibits binding affinity towards PPs presents both benefits and drawbacks with respect to its efficacy and toxicity. From this perspective, the molecular and physiological mechanisms underlying the binding of an anticancer drug to PPs must be studied as thoroughly as possible - both theoretically and empirically - to gather important data that can be used to better understand the ADME behaviour (Roberts et al., 2013). Interestingly, when administered to humans, BINI has a PP of 97.2% (EMA, 2023) and ENC of approximately 86% (Pfizer, 2023); therefore, the investigation of their PP binding behaviour is of paramount importance in the context discussed a few lines above.

The most prevalent protein in plasma, human serum albumin (HSA), is one of the proteins that has been the subject of the most intensive research. The liver produces HSA, which is exported as a single non-glycosylated chain and accumulates in the blood at a level of about 7.0×10^{-4} M. HSA is most recognised for its exceptional ligand binding ability, which serves as a depot for a range of substances that may be present in amounts far above those of their plasma solubility (Rabbani and Ahn, 2019). Due to its abundance in the bloodstream, HSA plays a significant role in the pharmacokinetics of many medicines, influencing both their efficacy and rate of delivery (Fasano et al., 2005). Especially for highly plasma-bound compounds such as the BRAFi ENC but also the MEKi BINI, the anticancer drug interactions with HSA are critical in oncology targeted therapy since the amount of the unbound drug fraction is strictly connected to the actual concentration of the drug at its biological target site. Focussing on drug-HSA interactions is important because HSA has emerged as a versatile carrier of therapeutic agents against diabetes, cancer, and infectious diseases, thereby acting as a drug delivery system. However, in some instances, HSA-drug interactions may have potentially harmful effect on patient health (Ghinea, 2021). As a result, obtaining precise information on the HSA binding properties of a given drug can play a pivotal role in a better understanding of its mode of action and its pharmacodynamics and pharmacokinetic characteristics (Wang et al., 2019a; Zhao et al., 2022). Drug-HSA binding studies can also be important from a theoretical and practical perspective because they help understand the mechanisms underlying drug bioavailability and elimination as well as the effects of different pathological conditions or medications on drug delivery and efficacy (Wang et al., 2019b). The interaction profile with HSA can actually be changed by the combination of BRAF/MEK inhibitors, and in those cases where the therapeutic windows are limited, this can have notable implication for the patient (Russi et al., 2022).

In this work, we present the results obtained from a combined experimental/computational approach aimed at investigating the binding properties of the two clinically approved BRAF and MEK inhibitors ENC and BINI to HSA. We conducted steady-state fluorescence (SSF) quenching experiments and isothermal titration calorimetry (ITC) to characterise the binding thermodynamics and kinetics of both anticancer drugs to HSA from an experimental perspective. Although competitive site marker displacement experiments and molecular simulations helped us in defining the binding site and the interaction mode of these two inhibitors with HSA, far-ultraviolet circular dichroism (far-UV CD), and synchronous fluorescence spectroscopy (SFS) were further used to investigate any conformation change that might be induced in the protein structure by drug binding.

2. Materials and methods

2.1. Reagents and chemicals

Globulin and fatty acid-free HSA (A1887) was obtained from Signa Aldrich Inc. (Saint Louis, MO, USA), while encorafenib, binimetinib, indomethacin, ketoprofen, and hemin were obtained from MedChemExpress (Monmouth, NJ, USA). All other reagents and chemicals (analytical grade) were also purchased from Sigma Aldrich.

2.2. Sample preparation and analytical procedures

A stock solution of HSA was prepared by dissolving a specific amount

of protein in phosphate buffer saline (PBS) with the following composition: 137 mM NaCl, 2.7 mM KCl, 10 mM Na_2HPO_4, and 1.8 mM KH_2PO_4 (25 °C; pH = 7.4), and the protein concentration was determined by UV spectroscopy using the value of 35,700 $M^{-1}cm^{-1}$ for the molar extinction coefficient at wavelength λ = 280 nm (Leggio et al., 2008; Pace et al., 1995). Similarly, stock solutions of ENC, BINI, IND, KET, and HEM were prepared in ethanol. All stock solutions were maintained in the dark at 4 °C.

2.3. Ultraviolet-Visible spectroscopy

The ultraviolet-visible (UV–Vis) absorption spectra of HSA, ENC, and BINI were recorded on a V-730 UV–Visible Spectrophotometer (Jasco, Japan) at room temperature (25 °C).

2.4. Steady-State fluorescence spectroscopy

All steady-state fluorescence (SSF) measurements were performed using a FP-8350 spectrofluorometer (Jasco, Japan) equipped with a thermostatic cell holder and a 1 cm quartz cell. The excitation wavelength (λ_{exc}) was set at 280 nm and the fluorescence spectra were recorded in the range 300 – 400 nm at three temperatures (25 °C, 31 °C and 37 °C) using 5/10 nm slit widths. During all fluorescence quenching titrations, the HSA concentration was kept fixed at 2 μM, while the concentrations of ENC and BINI were varied according to the following pattern: 1, 2, 3, 4, 5, 6, 10, 20, 40 μM. Each drug/protein solution was allowed to incubate for 2 h before recording the corresponding fluorescence spectrum. All fluorescence data were corrected for the inner filter effect according to the following equation (Lakowicz, 2006):

$$F_{corr} = F_{obs} \times 10^{(A_{exc}+A_{em})/2} \quad (1)$$

in which F_{corr} and F_{obs} are the corrected and observed fluorescence intensities, respectively, while A_{exc} and A_{em} are the absorption of the systems at the excitation (280 nm) and the emission (343 nm) wavelengths, respectively. Control experiments were carried out to check the influence of ethanol and pristine drugs. The solvent did not affect substantially the fluorescence spectra of HSA at all tested concentrations while both ENC and BINI have no significant emission in the range 300 – 450 nm at the same experimental conditions (data not shown).

2.5. Isothermal titration calorimetry studies

Thermodynamics of HSA/drug complex formation was investigated using isothermal titration calorimetry (ITC) experiments performed with a MicroCal PEAQ-ITC calorimeter (Malvern, UK) at 25 °C (cell volume = 208 μL). The sample cell was filled with a PBS solution of HSA at concentration of 20 μM while the syringe was filled with a 200 μM buffered solution of each inhibitor. Before each experiment, solutions and buffer were degassed for 30 min at room temperature. The titrations were carried out in 19 step-by-step injections of 2 μL volume under stirring at 750 rpm. Control experiments were used to measure unspecific heats (data not shown), which were then removed from the corresponding data set to provide the corrected integrated results. All experiments were run in triplicates. Data acquisition and analysis were performed using GraphPad Prism 8.0.0 for Mac (GraphPad Software, San Diego, California USA, www.graphpad.com).

2.6. Synchronous fluorescence spectroscopy

The synchronous fluorescence (SFS) spectra were recorded with scanning ranges Δλ = 60 nm (for tryptophan residues) and 15 nm (for tyrosine residues) (Zargar et al., 2022) in the absence of and in the presence of ENC or BINI. The excitation and emission slit widths were set at 5 nm and 10 nm, respectively while the scan speed was set at 100 nm/min. In each assay, HSA (2 μM) was titrated with ENC or BINI at concentrations ranging from 0 to 40 μM.

2.7. Far-UV circular dichroism spectroscopy

Far-UV circular dichroism (far-UV CD) spectra were recorded from 200 to 260 nm at a scan rate of 20 nm min^{-1} and at 25 °C on a J-1500 spectropolarimeter (Jasco, Japan) equipped with thermostatic cell holder and PML-534 FDCD detector. The path length cell was 0.2 cm, while step size and band width were set to 0.5 nm and 1 nm, respectively. The observed spectra were corrected for baseline (pure buffer solution), and the final CD curves are presented as the average of 3 accumulations. All spectra were visualized and analysed with Jasco Spectra Manager software. The fractional content of the secondary structure elements of the HSA, in the presence and absence of the two drugs, was calculated in the CD Multivariate SEE program using the standard calibration models.

2.8. Competitive site marker displacement experiments

Competitive site marker displacement studies were carried out with the three different HSA binding site markers indomethacin (IND), ketoprofen (KET) and hemin (HEM) - specific site markers for binding sites I, II, and III, respectively (Zhivkova, 2015). In these experiments, ENC or BINI (0–40 μM) were gradually added to a co-solution of HSA (2 μM) and a marker (2 μM), respectively, and the relevant fluorescence quenching data were collected following the same methodology described in *Section 2.4*.

2.9. Molecular simulations

The preparation of the molecular models was performed following a well-validated procedure (Russi et al., 2022). Briefly, the crystal structure of HSA was downloaded from the RCSB Protein Data Bank (Berman et al., 2000) (PDB ID 4k2c (Wang et al., 2013)), while the molecular models of ENC and BINI were built and optimised using the Avogadro software (Hanwell et al., 2012). The Autodock Vina software (Trott and Olson, 2010) was exploited for the docking studies of the HSA/ENC and HSA/BINI complexes. The search space for the docking computations was restricted to the subdomain IIA (Sudlow binding site I), in agreement with the results obtained from the fluorescence competition studies. All parameters were left with their default values, except the exhaustiveness parameter, which was increased to 25, and the number of solutions, which was set to 15. For the subsequent molecular dynamics (MD) experiments, the structure of the ligand/protein complexes characterized by the lowest-scoring energy were selected for both drugs. The UCSF Chimera software (Pettersen et al., 2004) was used to visualize the docking results, as well as to produce all of the molecular images.

Each intermolecular complex was then solvated by a cubic box of TIP3P water molecules (Jorgensen et al., 1983) and energy-minimized using a combination of MD techniques. 10 ns MD simulations at 25 °C were then employed for system equilibration, and further 50 ns MD simulations were run for data production. The analysis of the per-residue binding free energy deconvolution (PRBFED) of the enthalpic term (ΔH) was carried out using the molecular mechanics/generalised Boltzmann surface area (MM-PBSA) approach, while the computational analysis on the HSA structure in the presence or absence of drugs was performed with the cpptraj (Roe and Cheatham, 2013) module implemented in Amber 21 (Case et al., 2021). All simulations were carried our using Amber 21 running on the Marconi100 GPU/CPU supercomputer (CINECA, Bologna, Italy) and on our own CPU/GPU cluster.

3. Results and discussion

3.1. Steady-state fluorescence quenching of HSA

The SSF quenching of aromatic amino acids (Matyus et al., 2006; Sudlow et al., 1975) is a proficient approach for investigating the binding affinity and mechanism underlying ligand-protein interactions. The utilization of fluorescence quenching presents numerous advantages in comparison to other biophysical and biochemical methodologies for the examination of protein/ligand interaction (Dos Santos Rodrigues et al., 2023; Sridharan et al., 2014). For instance, quantitative measurements can be obtained as the fluorescence intensity is directly related to the quantity of fluorophores in a sample (Rabbani et al., 2015, 2014). In addition, fluorescence is subject to multiple factors that can be assessed independently or collectively, providing insights beyond the mere existence of a specific fluorophore, including its configuration and chemical environment.

Typically, upon HSA excitation at a wavelength (λ) of 280 nm, the fluorescence spectrum consists of tryptophan and tyrosine residues. Specifically, HSA exhibits a distinct emission peak at λ = 343 nm, and this characteristic fluorescence is attributed to the presence of a single tryptophan residue at position 214 (W214), located within Sudlow's site I in subdomain IIA of the protein. Upon gradual addition of ENC or BINI within the concentration range of 1 μM to 40 μM (in Fig. 1), the fluorescence intensity of HSA showed a gradual decline at 343 nm. However, the spectral characteristics and the position of the maximum emission peak remained unaltered. These evidences suggest conformational changes around the tryptophan residue of HSA as a result of the energy transfer between this amino acid and the kinase inhibitors and, consequently, to their binding against the serum protein.

To further examine the quenching mechanism involved in the interaction between ENC or BINI and the HSA, protein SSF quenching data obtained at three different temperatures (*i.e.*, 25 °C, 31 °C, and 37 °C) were analysed through the Stern-Volmer equation:

$$F_0/F = 1 + k_q\tau_0[Q] = 1 + K_{SV}[Q] \quad (2)$$

in which F_0 and F are the fluorescence peak intensities of the fluorophore (W214 of HSA) in the absence and presence of a quencher, respectively, k_q is the bimolecular quenching rate constant, τ_0 is the average lifetime of the protein (5.6 ns for HSA (Tayeh et al., 2009)), and [Q] is the concentration of the quencher (in this case ENC and BINI, respectively). Based on the K_{SV} values at different temperatures, the quenching mechanism can distinguish between static and dynamic modes (Rabbani et al., 2017). For the static quenching mode, also defined as binding-related quenching, K_{SV} values are predicted to decrease with increasing temperature, with the significant exception of entropy-driven binding (van de Weert and Stella, 2011). Furthermore, the static quenching mode is characterised by a rate constant value (k_q) above $2.06 \times 10^{10}\ M^{-1}s^{-1}$ (Lakowicz, 2006; Russi et al., 2022).

The Stern-Volmer plots for the HSA fluorescence quenching by ENC and BINI are reported in Fig. 1 (lower panels), while the corresponding calculated values of K_{SV} and k_q are listed in Table 1.

The findings presented in Table 1 demonstrate that the values of k_q, as determined by applying Eq. (2) to both drugs at the three temperatures, fall within the range of $10^{12}\ M^{-1}s^{-1}$. This indicates that the interactions between ENC/HSA and BINI/HSA are governed by a static quenching mechanism. It is worth to note that the k_q values, and consequently the K_{SV} values, exhibit an inverse correlation with temperature in the ENC/HSA complex. However, in the BINI/HSA complex, the opposite trend is observed, with k_q and K_{SV} increasing as the temperature increases (see Fig. 1 and Table 1). This observation gives rise to the hypothesis that although a quenching mechanism induced by the ligand remains operative, entropy might play a substantial role in the

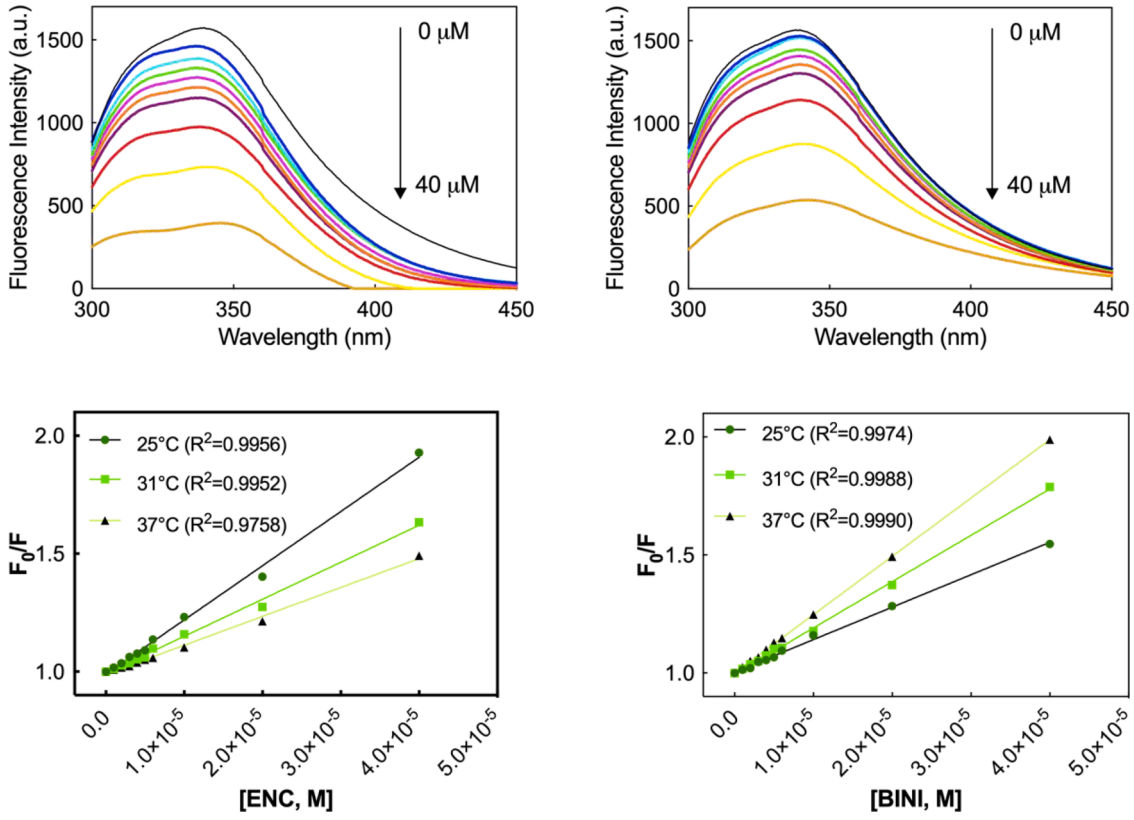

Fig. 1. (Top panel) Steady-state fluorescence quenching of HSA (2 μM) in the presence of increasing concentrations (0–40 μM) of ENC (left) and BINI (right) (PBS buffer, pH = 7.4, T = 25 °C, and λ_{exc} = 280 nm). (Bottom panel) Stern-Volmer plots for HSA fluorescence quenching induced by ENC (left) and BINI (right) at three different temperatures (25 °C, 31 °C, and 37 °C).

Table 1
Stern-Volmer constants (K_{SV}) and bimolecular quenching rate constants (k_q) for HSA tryptophan fluorescence quenching by ENC and BINI at different temperatures.

ENC			BINI		
T (°C)	K_{SV} (10^4 M^{-1})	k_q (10^{12} $M^{-1}s^{-1}$)[a]	T (°C)	K_{SV} (10^4 M^{-1})	k_q (10^{12} $M^{-1}s^{-1}$)[a]
25	2.30 ± 0.07	3.89	25	1.38 ± 0.06	2.33
31	1.57 ± 0.04	2.66	31	1.96 ± 0.06	3.33
37	1.23 ± 0.08	2.08	37	2.47 ± 0.09	4.19

[a] As mentioned in the text, here the value of $\tau_0 = 5.6$ ns for HSA was adopted for the calculation of k_q, in agreement with our previous works (Russi et al., 2022).

formation and stabilisation of the BINI/HSA complex.

3.2. Binding parameters and thermodynamic parameters analysis

The assumption that HSA features n independent ligand binding sites can be confirmed by the detection of static quenching. Accordingly, the values of binding constant (K_a) and the corresponding values of n can be calculated using the double-logarithmic version of the Stern-Volmer equation (Bi et al., 2004):

$$\log(F_0 - F)/F = n \log K_a - n \log[1 / ([L_T] - (F_0 - F)[P_T]/F_0)] \quad (3)$$

where F_0 and F are the same quantities of Eq. (2), n denotes the number of protein binding site, K_a is the binding constant, while $[L_T]$ and $[P_T]$ are the total ligand and the total protein concentration, respectively.

The determination of K_a and n values for both drug/HSA complexes can be obtained by analysing the linear correlation between the two logarithmic terms in Eq. (3), as depicted in Fig. 2 (upper panel). The results of the calculations for the binding affinity and the number of binding sites are presented in Table 2. The values of n for both inhibitors at all three temperatures were close to 1, suggesting the presence of only one preferential binding site for ENC and BINI within the HSA structure.

Furthermore, within the temperature range examined, both ENC and BINI demonstrated similar serum protein capacities, as indicated by the comparable K_a values on the order of 10^4 M^{-1} (Table 2). This suggests a modest level of affinity between HSA and the inhibitors, which could be advantageous for the transport and release of the drugs by this plasma protein. Furthermore, opposite trends are observed in the temperature-dependant conduct of the K_a values in the two scenarios; specifically, the interactions between ENC and HSA, indeed, showed a usual, inverse correlation between K_a and temperature. Conversely, the complex of BINI/HSA exhibited a less common direct correlation between K_a values and temperature. Thus, these results further support the hypothesis that the association between the MEK inhibitor and HSA is primarily driven

Table 2
Binding parameters of HSA with ENC and BINI derived from fluorescence quenching data using Eq. (3) and from the vant' Hoff plots (Fig. 2, lower panels). The values of ΔG are derived from the ΔH and ΔS values obtained from the corresponding van't Hoff plots (Eq. (4)) using Eq. (5).

Ligand	T (°C)	K_a (10^4 M^{-1})	n (-)	ΔH (kcal/mol)	ΔS (cal/mol K)	ΔG (kcal/mol)
ENC	25	2.31 ± 0.07	1.08			−5.93
	31	1.85 ± 0.05	1.03	−4.09	+6.19	−5.97
	37	1.77 ± 0.06	1.05			−6.01
BINI	25	2.06 ± 0.04	1.09			−5.87
	31	2.15 ± 0.03	1.07	+2.01	+26.5	−6.03
	37	2.35 ± 0.05	1.04			−6.19

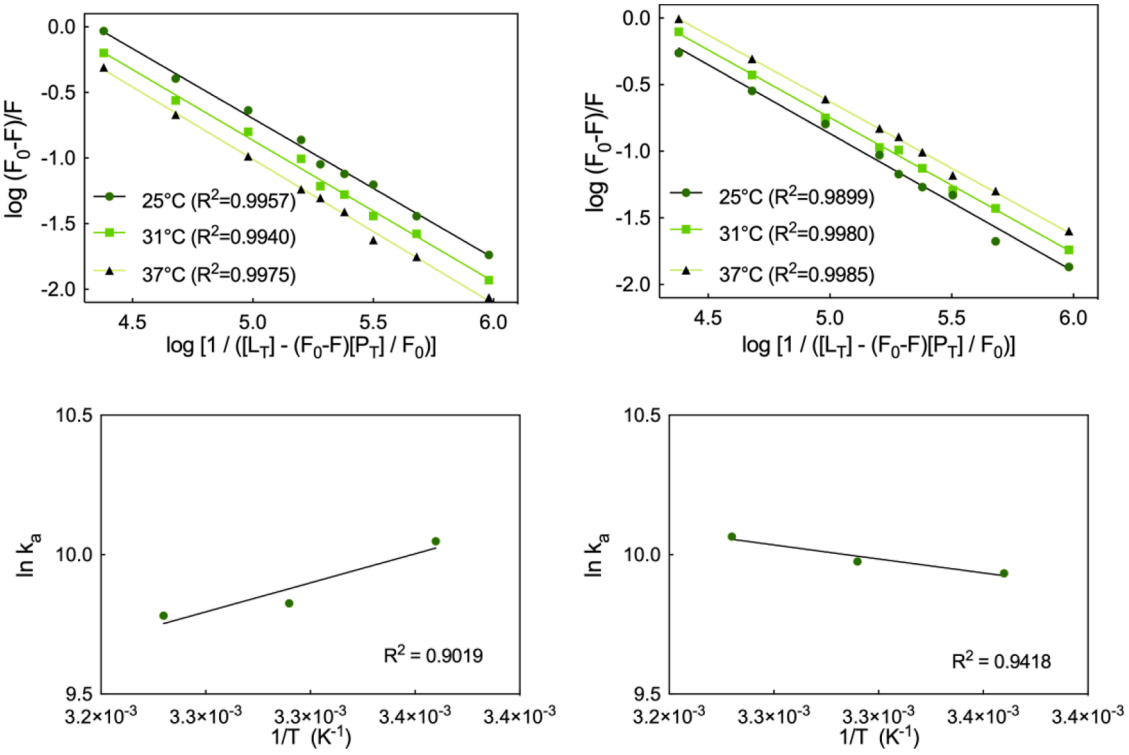

Fig. 2. (Upper panel) Plots of log (F_0-F) *vs.* log [1/([L_T])-(F_0-F)[P_T])/(F_0)]) for HSA fluorescence quenching by ENC (left) and BINI (right) at three different temperatures (25 °C, 31 °C, and 37 °C). (Bottom panel) The van't Hoff plots (lnK_a *vs* 1/T, see Eq. (6)) for ENC/HSA (left) and BINI/HSA (right) binding interactions.

by the entropy contribution.

Thermodynamic data can be used to estimate and describe the intermolecular interactions that contribute to the stability of ligand-protein complexes. Hydrophobic interactions, van der Waals forces, electrostatic interactions, and hydrogen bonds are the predominant intermolecular forces that have been identified as stabilising a typical ligand-protein association process (Ross and Subramanian, 1981). Consequently, to get into more detail about the complete thermodynamic nature of the binding interactions of the ENC/HSA and BINI/HSA complexes, the variation of the binding enthalpy (ΔH), entropy (ΔS) and free energy (ΔG) were obtained from the van't Hoff equation (Table 2) by exploiting the linear relationship between $\ln K_a$ and $1/T$ as follows:

$$\ln K_a = -\Delta H/RT + \Delta S/R \quad (4)$$

where R is the universal gas constant (1.987 cal/mol K). Accordingly, by plotting $\ln K_a$ *vs.* $1/T$, the values of ΔH and ΔS can be directly obtained from the slope and the intercept of the relevant linear fits (Fig. 2, lower panels).

Finally, the Gibbs free energy change (ΔG) of the binding process was calculated for each drug/protein complex by replacing the corresponding ΔH and ΔS values in the following equation:

$$\Delta G = \Delta H - T\Delta S \quad (5)$$

The negative values of ΔG listed in Table 2 indicate that the binding process between ENC and BINI against HSA is spontaneous and thermodynamically favourable at all temperatures. In the case of the BINI/HSA complex, the positive ΔH value (+2.01 kcal/mol) clearly denotes that the binding event is endothermic, which is further corroborated by the rise in the K_a value as the temperature increases (Table 2). The large positive ΔS value (+26.5 cal/(mol K) suggests that hydrophobic interactions play a significant role in stabilizing this complex (Ross and Subramanian, 1981). Consequently, as endothermic apolar interactions are strengthened with increasing temperature, it is plausible to consider the involvement of strong hydrophobic interactions between BINI and HSA. In contrast, the binding mechanism in the complex between the BRAFi ENC and the serum protein is driven by a favourable enthalpic contribution (ΔH = −4.09 kcal/mol, Table 2). At the same time, however, the positive entropy change (ΔS = +6.19 cal/(mol K)) value suggests that the binding of ENC to HSA is stabilized by a balanced combination of hydrogen bonding/polar interactions and hydrophobic forces.

3.3. ITC binding analysis

During recent decades, ITC has become widely recognized as the preferred method for analysing intermolecular and/or intramolecular interactions. ITC is a biophysical method that is known for its high sensitivity and is widely regarded as one of the most precise techniques for obtaining a comprehensive thermodynamic characterization of binding events in solution. This method enables the direct measurement of the enthalpy change occurring in a reactive system as a function of the injected reactant quantity (Saboury, 2006; Santos et al., 2023; Su and Xu, 2018). Basically, ITC can simultaneously provide the three principal thermodynamic parameters (ΔH, ΔS and ΔG), along with the binding affinity constant K_a and the reaction stoichiometry (number of binding sites) n for every association/dissociation event.

Accordingly, ITC experiments were initially performed to determine the binding thermodynamics of BINI and ENC to HSA at 25 °C, and the results are shown in Fig. 3 and Table 3.

The data obtained from ITC support the spontaneous formation of both drug-protein complexes with a 1:1 stoichiometry, as shown in Fig. 3 and Table 3. Specifically, for the ENC/HSA complex, the

Table 3
Thermodynamic parameters (ΔH, $T\Delta S$, ΔG, n, K_a) involved in the formation of drug/HSA complexes as obtained from ITC experiments at 25 °C. All ITC experiments were in run in triplicate. Errors on ΔH are within 10%.

Ligand	K_a (10^4 M^{-1})	n (-)	ΔH (kcal/mol)	$T\Delta S$ (kcal/mol)	ΔS (cal/mol)	ΔG (kcal/mol)
ENC	2.14 ± 0.18	1.09 ± 0.11	−4.24 ± 0.08	+1.67	+5.60	−5.91
BINI	1.48 ± 0.21	1.13 ± 0.15	2.53 ± 0.16	+8.22	+27.6	−5.69

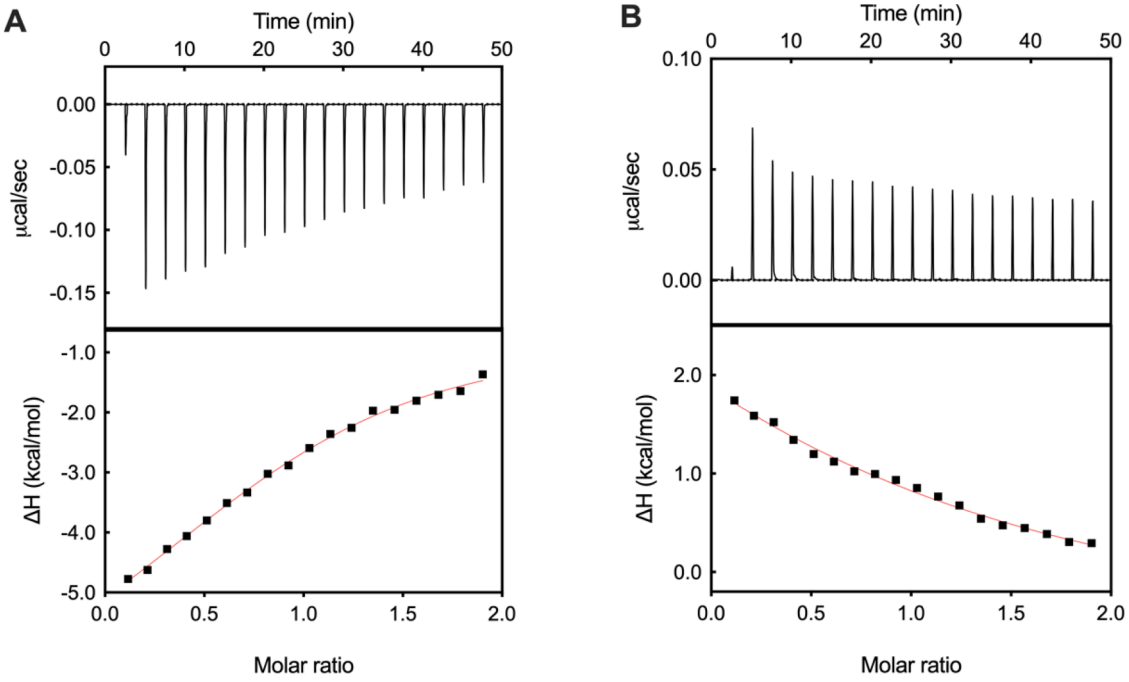

Fig. 3. ITC raw data (upper panels) and plots of the integrated ITC data (bottom panels) for the interaction between ENC (A) and BINI (B) with HSA at 25 °C ([HSA] = 20 µM, PBS buffer, pH =7.4). The solid red line corresponds to the data fitting with the one-site (1:1 binding stoichiometry) isothermal binding model.

integrated heat curve yielded the following values: $K_a = 2.14 \times 10^4\ M^{-1}$, $\Delta G = -5.91$ kcal/mol, and $n = 1.09$, while for the BINI/HSA ensemble the corresponding values were $K_a = 1.48 \times 10^4\ M^{-1}$, $\Delta G = -5.69$ kcal/mol, and $n = 1.13$ (Table 3). These values are not only excellently in agreement with those estimated from the corresponding SSF quenching data (Table 2) but, furthermore, they validate the distinct roles played by the interaction forces in facilitating the association between the two inhibitors and HSA, as deduced from SSF quenching data analysis.

In the case of ENC/HSA binding, Table 3 shows that the enthalpy variation upon binding is negative (−4.24 kcal/mol) and greater than the corresponding, positive entropic TΔS term (+1.67 kcal/mol). This indicates that the association process between ENC and HSA is driven by enthalpy, promoted by hydrogen bonding/polar interactions, and further stabilised by a weak network of hydrophobic interactions. On the contrary, in the case of the alternative BINI/HSA complex, both ΔH and TΔS are positive, suggesting that the binding between the protein and the MEKi is primarily governed by hydrophobic interactions. In addition, the entropy change involved in the formation of this complex (+8.22 kcal/mol, Table 3) is significantly greater than the corresponding ΔH contribution, ultimately resulting in a thermodynamically spontaneous binding event (*i.e.*, $\Delta G < 0$).

3.4. Synchronous fluorescence spectra of HSA in presence of ENC and BINI

Synchronous fluorescence spectroscopy offers numerous advantages over conventional FS, including simple spectra, high sensitivity/selectivity, spectral bandwidth reduction, and low interference. Acquiring SFS spectra is accomplished by simultaneously scanning the excitation and emission monochromators of a spectrofluorometer, while keeping the wavelength difference ($\Delta\lambda$) between them constant. In particular, SFS can provide information on the molecular microenvironment surrounding a chromophore and measuring the possible shift in synchronous maximum wavelength (λ_{max}) is now a standard method to investigate the environment of amino acid residues. At small values (*i.e.*, $\Delta\lambda = 15$ nm), the SFS spectra of a mixture of tyrosine (Y) and tryptophan (W) are characteristic of Y, while at large values (*i.e.*, $\Delta\lambda = 60$ nm), the spectra resemble those of W (Byadagi et al., 2017).

Fig. 4 presents the SFS spectra of ENC and BINI when interacting with HSA at wavelength shifts $\Delta\lambda$ of 15 nm and 60 nm, respectively. At first sight, the fluorescence intensity of the four spectra exhibited a consistent decrease upon the addition of compounds, thereby corroborating the results obtained from the SSF quenching assay.

Nevertheless, certain dissimilarities in the interplay between the two inhibitors and the serum protein can be emphasized. In fact, the spectra of the ENC/HSA complex exhibited a red shift in the λ_{max} value at both $\Delta\lambda$ values, as shown in the left panels of Fig. 4. This observation suggests that ENC has the capability to enhance the polarity around both Y and W. In contrast, in the BINI/HSA system a slight red shift in λ_{max} is observed only at $\Delta\lambda$ =60 nm (Fig. 4, right panels), indicating that the MEKi inhibitor only affects the microenvironment surrounding the W residue within the HSA structure.

3.5. Structural analysis of the ENC/HSA and BINI/HSA complexes

3.5.1. Circular dichroism spectroscopy

Circular dichroism is a highly sensitive methodology utilised to monitor changes in the conformation of a protein (Greenfield, 2006). The CD spectrum of pure HSA displays two negative bands ($\lambda = 208$ nm and 222, nm, respectively), that are indicative of the α-helical structures of the protein. The former band results from the exciton splitting of electronic transitions from the peptide amide nonbonding orbital π_{nb} to the antibonding orbital π^*, while the latter band is due to the electronic transition from an oxygen lone pair orbital n to the π^* orbital. To investigate the potential impact of ENC and BINI binding on the secondary structure of this important serum protein, far-UV CD spectroscopy measurements were performed on the pristine HSA as well as its presence in the presence of each inhibitor at 25 °C and at three different

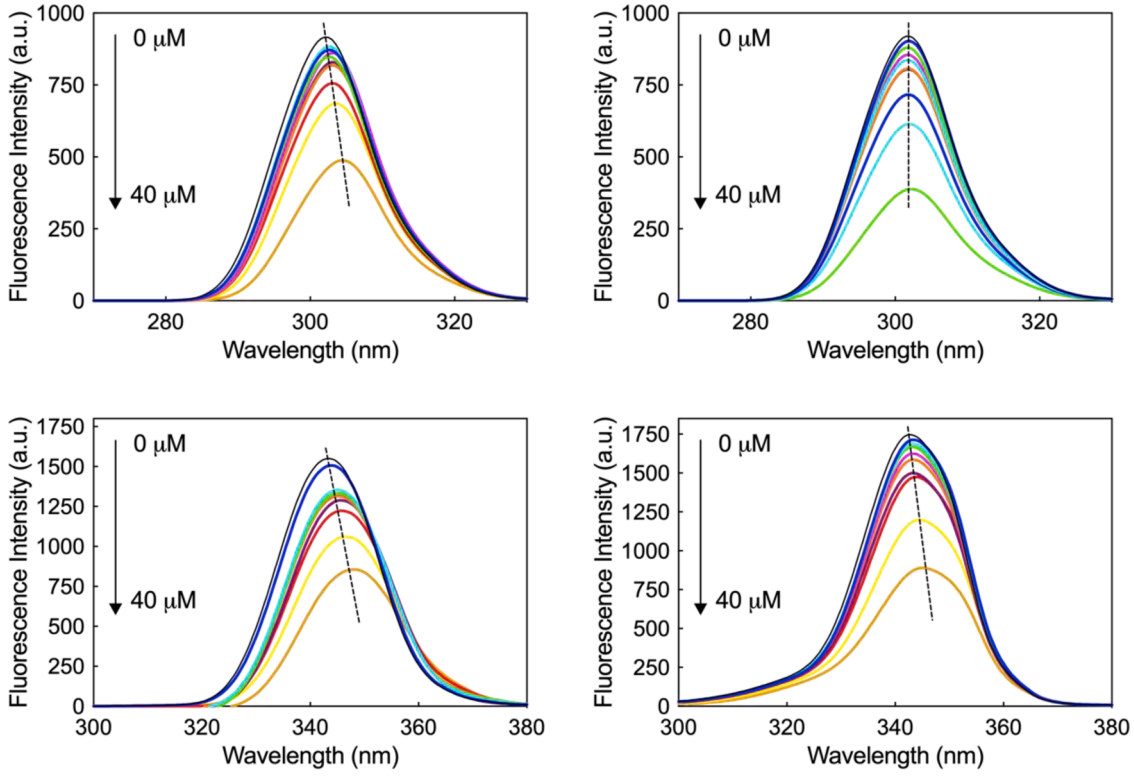

Fig. 4. The synchronous fluorescence spectra of HSA (2 μM) at $\Delta\lambda = 15$ (upper panels) and 60 nm (bottom panels) in the presence of ENC (left) or BINI (right) at 25 °C.

drug/protein molar ratios (0.5, 1, and 2), as shown in Fig. 5.

Intriguingly, for the ENC/HSA and BINI/HSA systems the CD spectra did not exhibit any noteworthy alterations in comparison to HSA alone, except for the complex with the BRAFi at its maximum concentration (as shown in Fig. 5). However, the intensities of the corresponding CD bands exhibited only a minor decrease in signal, and there was no observable displacement of the band minima following the addition of ENC. This indicates that, even in this scenario, the secondary structure of the protein is only slightly affected. To corroborate these evidences, we compared the estimated content of α-helical motifs (% α-helix) of free and drug-bound HSA using the two established equations:

$$\mathrm{MRE}_{208} = \text{observed CD (mdeg)} / 10 C_{\mathrm{p}} n l \quad (6)$$

$$\%\ \alpha - \text{helix} = \left(, -\mathrm{M}, \mathrm{RE}_{,208,} - 4,000, /33,000, -40,00\right) \times\ 100 \quad (7)$$

in which MRE is the value of the mean residue ellipticity at λ = 208 nm (expressed in deg cm^2 $dmol^{-1}$), *Cp* is the molar concentration of HSA (2 μM), *n* denotes the number of amino acids in the protein primary sequence (585 for HSA), *l* is the path length of the CD cell (0.1 cm), while 33,000 and 4000 (in deg cm^2 $dmol^{-1}$) correspond to the MRE_{208} values of pure α-helical and β-sheet/random coil structures, respectively.

The values shown in Table 4 agree with literature reports (Jiao et al., 2019; Juarez et al., 2009; Tang et al., 2018) and confirm that the α-helical composition of HSA remained substantially unchanged upon binding of either drug at every concentration tested, the only exception being observed for the BRAFi at the highest drug/protein molar ratio, for which a slight decrease of the HSA a-helical content (56.1%) was estimated.

3.5.2. Drug displacement experiments

Site-selective probes were utilised to conduct displacement experiments aimed at identifying the specific binding site for ENC and BINI in the structure of human serum albumin. The HSA subdomains IIA and IIIA comprise Sudlow's site I and II, respectively, which have been categorised as possessing high affinity for a diverse range of pharmaceutical compounds (De Simone et al., 2021; Fasano et al., 2005; Sudlow et al., 1975). Furthermore, there have been reports indicating that the HSA IB subdomain encompasses an additional binding cavity, which is referred to as the drug binding site III (Zsila, 2013). In this study, we purposely selected three active molecules - specifically indomethacin (IND), ketoprofen (KET), and hemin (HEM), that are known to be specific site markers for the protein binding sites I, II, and III, respectively – and recorded the fluorescence emission spectra obtained during the titration of premixed solutions of HSA and each site marker with progressively increasing concentrations of ENC or BINI. Utilizing Eq. (3), we performed data fitting to assess the impact of individual site markers on the binding of the BRAFi and MEKi to HSA through the determination of the relevant binding constants K_a, as shown in Table 5.

As evidenced by Table 5, the K_a values of ENC and BINI in the presence of IND against albumin are significantly reduced compared to those obtained with the free protein. However, their affinity remains largely unchanged in the presence of the alternative site markers KET and HEM. To corroborate these findings, investigations were carried out to examine the competitive interplay between ENC and BINI with respect to their binding to HSA. As evidenced by the data presented in Table 5, a notable disparity in binding capacity is apparent between the isolated inhibitor/HSA system and the system in the presence of a constant concentration of the alternative drug. As a result, the two antitumor drugs exhibit similar ability to contend for occupancy at the same binding site within the HSA structure, where they mutually hinder each other. Collectively, the results obtained suggest that there is a displacement interaction between ENC and BINI during their binding process with HSA, and that the Sudlow's binding site I, situated in the subdomain IIA, is the probable binding cavity for ENC and BINI on HSA.

Table 4
α-helical content (% α-helix, ± standard errors) of HSA in the absence and in presence of ENC and BINI calculated from CD experiments at 25 °C using Eqs. (6) and (7).

Ligand	Ligand/HSA Molar Ratio	α-helix (%)
–	–	58.0 ± 0.3
ENC	0.5	58.3 ± 0.2
	1	58.0 ± 0.1
	2	56.1 ± 0.4
BINI	0.5	58.4 ± 0.1
	1	57.8 ± 0.1
	2	57.7 ± 0.2

Table 5
Binding constants for ENC and BINI to HSA derived from fluorescence quenching data obtained at 25 °C in the absence and presence of IND, KET, HEM using Eq. (3).

	ENC	BINI
Site Marker	K_a (10^4 M^{-1})	K_a (10^4 M^{-1})
none	2.31 ± 0.07	2.06 ± 0.04
IND	1.86 ± 0.04	1.57 ± 0.07
KET	2.03 ± 0.03	2.37 ± 0.11
HEM	2.01 ± 0.09	2.35 ± 0.12
Competitor	K_a (10^4 M^{-1})	K_a (10^4 M^{-1})
ENC	–	1.26 ± 0.10
BINI	1.35 ± 0.09	–

3.5.3. Molecular simulations studies of HSA binding with ENC and BINI

To obtain detailed molecular information on the interactions between ENC and BINI with HSA, we exploited the results obtained from displacement experiments (see *Section 3.5.2*) to perform molecular dynamics (MD) simulations of the BRAFi and the MEKi within the IIA protein subdomain (Fig. 6). Molecular docking was employed to position

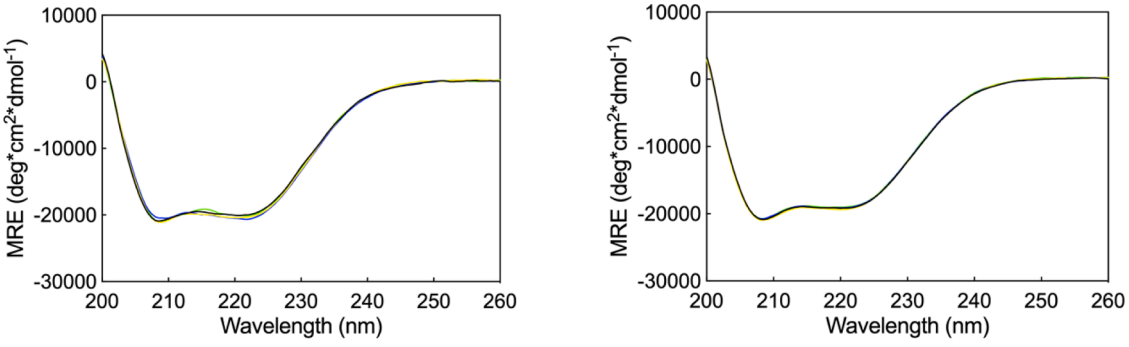

Fig. 5. Far-UV CD spectra of HSA alone (black line) and in the presence of ENC (left) and BINI (right) in a molar ratio of 0.5 (yellow line), 1 (green line) and 2 (blue line). The CD experiment were carried out in PBS buffer solution, at 25 °C and at [HSA] = 2 μM.

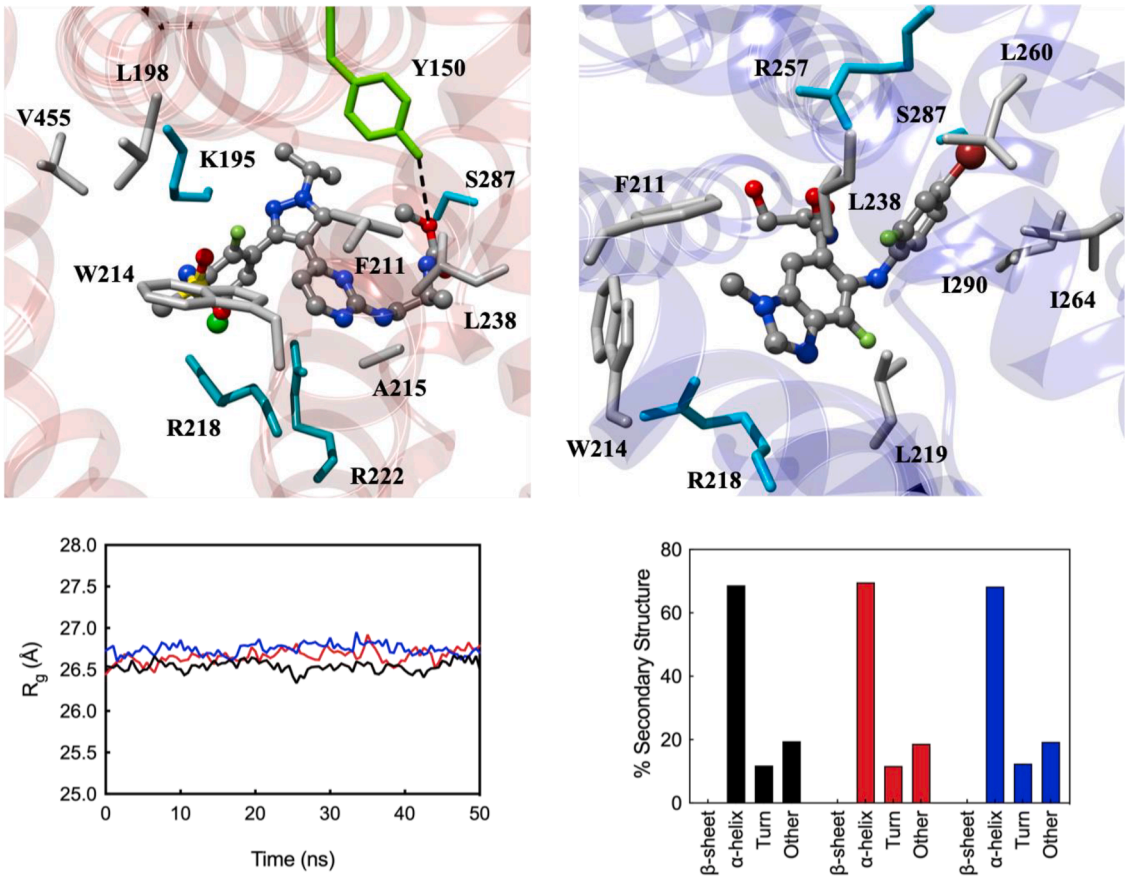

Fig. 6. (Upper panels) Binding of ENC (left) and BINI (right) in the Sudlow's site I (subdomain IIA) of HSA. The two compounds are depicted as atom-coloured sticks (C, grey; O, red; N, blue; S, yellow; F, light green; Cl, forest green), while the protein is shown in transparent ribbons. HSA residues mainly involved in drug binding are highlighted and labelled. Hydrogen bonds are indicated by broken black lines and labelled. Hydrogen atoms, water molecules, ions, and counterions are not shown for clarity. (Lower panels) Plot of the radius of gyration (left) as a function of the simulation time for free HSA (black) and in complex with ENC (red) and BINI (blue), respectively. Plot of the HSA secondary structure estimation (right) averaged during the 50 ns of MD simulation for free HSA (black) and in complex with ENC (red) and BINI (blue), respectively.

ENC and BINI within the experimentally identified binding pocket. The most favourable conformation determined by the docking algorithm was used for subsequent MD simulations. This computational approach was utilized to qualitatively describe the binding mechanism of the HSA/ENC and HSA/BINI complexes and to assess any potential effects of the drugs on the protein structure.

Starting the analysis with BRAF inhibitor, the ENC/HSA complex is characterized by the presence of a permanent hydrogen bond between the sp3 carbamate oxygen atom and the hydroxylic group of the side chain of Y150 of HSA (Fig. 6, upper left). Additionally, positive and stabilizing polar interactions are highlighted between the hydrophilic side chains of K195 and S287 with the pyrazol portion of the drug and the carbamate moiety, respectively. A further stabilization of the ENC/HSA binding is provided by the presence of stable π-cation interactions between the chloro- and fluoro-substituted aromatic ring of the drug and the positively charged side chains of R218 and R222. Finally, during the entire timeframe of the MD simulation, a network of hydrophobic and van der Waals interactions are detected between the apolar functional groups of ENC and the lipophilic side chains of the albumin residues L198, F211, W214, A215, L238, and V455. Accordingly, the binding thermodynamics described by fluorescence spectroscopy and ITC experiments (see *Sections 3.2* and *3.3*) are confirmed, where a predominantly enthalpic character for the interactions between ENC and HSA emerges. Moreover, the direct interactions highlighted with Y150 and W214 corroborate the results obtained with the SFS technique (see *Section 3.4*).

Moving to the complex between HSA and the MEK inhibitor, it can be observed from the upper right panel in Fig. 6 that, although the two drugs share the same binding pocket, the network of stabilizing interactions is quite dissimilar. During the corresponding MD simulation, in fact, the 4-bromo-2-fluorobenzene ring of BINI is nestled in a hydrophobic pocket delimited by the side chains of HSA residues L238, L260, I264 and I290, while the benzimidazole portion is strongly stabilized by hydrophobic contacts with the side chains of F211, W214, and L219. Only other weak polar interactions are detected in the binding cavity between the hydroxy ethoxy moiety of BINI with R257 and S287 and the imidazolic nitrogen atoms with the charged side chain of R218. In agreement with the experimental binding thermodynamics data derived from fluorescence spectroscopy and calorimetric analysis (see *Sections 3.2* and *3.3*), the interactions described above mainly characterize the binding between BINI and HSA, supporting a binding mode primarily driven by the entropic contribution.

MD simulations were also performed to study any structural changes in HSA caused by binding with the two drugs. In particular, structural analysis was used to calculate important parameters of the protein such as the radius of gyration (R_g) and the percentage of secondary structure (Fig. 6, bottom panels). R_g provides an indication of the compactness of the structure and allows to highlight dimensional changes caused by the presence of an external molecule on a macromolecule structure (Baig et al., 2019). On the other hand, the percentage of secondary structure allows for a direct comparison with the results obtained from spectroscopic techniques (see *Section 3.5*). In summary, the average value of R_g during the MD simulations of the isolated serum protein was 26.54 ± 0.06 Å, in accordance with values obtained from previous studies (Baig

et al., 2019; Gurung et al., 2022; Mohseni-Shahri et al., 2016). For the ENC/HSA and BINI/HSA complexes, the R_g values were 26.67 ± 0.08 Å and 26.75 ± 0.07 Å, respectively (Fig. 6, bottom left panel). This result confirmed that the compactness and the folding state of HSA remain practically unchanged upon binding with the inhibitors, as indicated by circular dichroism experiments. Further confirmation of the CD experiments emerged from the estimation percentages of secondary structure calculated for both molecular systems and compared to the values of the pristine protein (Fig. 6, bottom right panel). The secondary structure of HSA, indeed, was essentially not influenced by the inclusion of ENC or BINI into their corresponding binding pockets.

4. Conclusions

In this study, we exploited a comprehensive strategy that integrated both experimental methodologies and molecular simulation techniques to examine how the binding process occurs between human serum albumin and two anticancer drugs, namely encorafenib and binimetinib, which represent one of the most effective combination treatments for melanoma. In aggregate, CD spectroscopy allowed for the characterization of the secondary structure in the presence and absence of the drugs. The structure observed in the absence of the ligands is consistent with literature data while the interaction with ENC or BINI did not result in any significant structural modifications on HSA. The results from fluorescence studies and calorimetric analysis indicate that both ENC and BINI bind to Sudlow's site I, subdomain IIA of the protein with moderate, similar affinities, but through different mechanisms. Specifically, the ENC/HSA association is primarily driven by enthalpy, promoted by the formation of intermolecular hydrogen bonds and additional π- and nonpolar interactions that enhance the stability of the corresponding complex. On the other hand, the binding of BINI to HSA is predominantly influenced by entropy contribution, driven by a robust network of hydrophobic interactions. In conclusion, the present research offers valuable perspectives on the underlying binding mechanism of ENC and BINI towards the human serum albumin and improves understanding of their transport and delivery in the blood and, in turn, of their pharmacokinetics profile. The results of this work could be also valuable for the improvement of therapeutic potential of the ENC/BINI combination treatment in melanoma by supporting the design and optimization of its dosage necessary to achieve the appropriate anticancer effect.

Availability of data and material

The data that support the findings of this study are included in this published article.

CRediT authorship contribution statement

Gabriele Cavalieri: Investigation, Data curation, Validation, Visualization, Writing – original draft. **Giulia Cilurzo:** Investigation, Data curation, Visualization. **Lorenzo Pettorosso:** Investigation, Data curation, Visualization. **Andrea Mansueto:** Investigation, Data curation, Visualization. **Erik Laurini:** Conceptualization, Supervision, Project administration, Writing – review & editing, Funding acquisition. **Sabrina Pricl:** Conceptualization, Writing – review & editing, Supervision, Project administration, Funding acquisition.

Declaration of Competing Interest

All authors have no conflicts of interest and no competing interest to declare.

Data availability

Data will be made available on request.

Acknowledgement

We wish to acknowledge the generous financial support from the Italian Association for Cancer Research (AIRC, grant "Novel hot-spot mutations in BCR-ABL1: role in resistance to CML target therapy - IG17413" to SP), the Friuli Venezia Giulia Region (REFVG, grant "Study of the oncogene B-Raf and its mutation for the selection of melanoma patients eligible for targeted therapies with specific inhibitors - No-Mel" to SP), and the Fondazione Cassa di Risparmio di Trieste (Fondazione CRTrieste, grant "Far-UV CD spectroscopy in translational medicine" to SP). SP, EL and GC acknowledge access to supercomputing resources and financial support from ICSC – Centro Nazionale di Ricerca in High-Performance Computing, Big Data, and Quantum Computing (Spoke 7, WP4 (Pilot applications), T2.8 (Development and optimization of HPC-based integrated workflows based on flagship codes for personalized (nano)medicine) and CINECA, funded by European Union – NextGenerationEU.

References

ACS, 2023. Stages of Melanoma Skin Cancer. American Cancer Society. https://www.cancer.org/cancer/melanoma-skin-cancer/detection-diagnosis-staging/melanoma-skin-cancer-stages.html. Accessed 20 June 2023.

Baig, M.H., Rahman, S., Rabbani, G., Imran, M., Ahmad, K., Choi, I., 2019. Multi-spectroscopic characterization of human serum albumin binding with cyclobenzaprine hydrochloride: insights from biophysical and in silico approaches. Int. J. Mol. Sci. 20 https://doi.org/10.3390/2Fijms20030662.

Berman, H.M., Westbrook, J., Feng, Z., Gilliland, G., Bhat, T.N., Weissig, H., Shindyalov, I.N., Bourne, P.E., 2000. The Protein Data Bank. Nucleic. Acids. Res. 28, 235–242. https://doi.org/10.1093/nar/28.1.235.

Bi, S.Y., Ding, L., Tian, Y., Song, D.Q., Zhou, X., Liu, X., Zhang, H.Q., 2004. Investigation of the interaction between flavonoids and human serum albumin. J. Mol. Struct. 703, 37–45. https://doi.org/10.1016/j.molstruc.2004.05.026.

Byadagi, K., Meti, M., Nandibewoor, S., Chimatadar, S., 2017. Investigation of binding behaviour of procainamide hydrochloride with human serum albumin using synchronous, 3D fluorescence and circular dichroism. J. Pharm. Anal. 7, 103–109. https://doi.org/10.1016/j.jpha.2016.07.004.

Case, D.A., Belfon, H.M.A., Ben-Shalom, I.Y., Berryman, J.T., Brozell, S.R., Cerutti, D.S., Cheatham III, T.E., Cisneros, G.A., Cruzeiro, V.W.D., Darden, T.A., Duke, R.E., Giambasu, G., Gilson, M.K., Gohlke, H., Goetz, A.W., Harris, R., Izadi, S., Izmailov, S. A., Kasavajhala, K., Kaymak, M.C., King, E., Kovalenko, A., Kurtzman, T., Lee, T.S., LeGrand, S., Li, P., Lin, C., Liu, J., Luchko, T., Luo, R., Machado, M., Man, V., Manathunga, M., Merz, K.M., Miao, Y., Mikhailovskii, O., Monard, G., Nguyen, H., O'Hearn, K.A., Onufriev, A., Pan, F., Pantano, S., Qi, R., Rahnamoun, A., Roe, D.R., Roitberg, A., Sagui, C., Schott-Verdugo, S., Shajan, A., Shen, J., Simmerling, C.L., Skrynnikov, N.R., Smith, J., Swails, J., Walker, R.C., Wang, J., Wang, J., Wei, H., Wolf, R.M., Wu, X., Xiong, Y., Xue, Y., York, D.M., Zhao, S., Kollman, P.A., 2021. Amber 2021. University of California, San Francisco.

Dankner, M., Rose, A.A.N., Rajkumar, S., Siegel, P.M., Watson, I.R., 2018. Classifying BRAF alterations in cancer: new rational therapeutic strategies for actionable mutations. Oncogene 37, 3183–3199. https://doi.org/10.1038/s41388-018-0171-x.

De Simone, G., di Masi, A., Ascenzi, P., 2021. Serum Albumin: a Multifaced Enzyme. Int. J. Mol. Sci. 22 https://doi.org/10.3390/ijms221810086.

Dhillon, A.S., Hagan, S., Rath, O., Kolch, W., 2007. MAP kinase signalling pathways in cancer. Oncogene 26, 3279–3290. https://doi.org/10.1038/sj.onc.1210421.

Dos Santos Rodrigues, F.H., Delgado, G.G., Santana da Costa, T., Tasic, L., 2023. Applications of fluorescence spectroscopy in protein conformational changes and intermolecular contacts. BBA Adv. 3, 100091 https://doi.org/10.1007/s12154-013-0094-5.

ECIS, 2023. European Cancer Information System. 'Melanoma_cancer_en.pdf'. https://ecis.jrc.ec.europa.eu. Accessed 15 June 2023.

EMA, 2023. European Medicines Agency. Withdrawal-assessment-report-balimek-binimetinib_en.pdf. https://www.ema.europa.eu/en/documents/withdrawal-report/withdrawal-assessment-report-zioxtenzo_en.pdf. Accessed 31 May 2023.

Fasano, M., Curry, S., Terreno, E., Galliano, M., Fanali, G., Narciso, P., Notari, S., Ascenzi, P., 2005. The extraordinary ligand binding properties of human serum albumin. IUBMB Life 57, 787–796. https://doi.org/10.15216540500404093.

Ghinea, N., 2021. Anti-angiogenic therapy: albumin-binding proteins could mediate mechanisms underlying the accumulation of small molecule receptor tyrosine kinase inhibitors in normal tissues with potential harmful effects on health. Diseases 9. https://doi.org/10.3390/diseases9020028.

Greenfield, N.J., 2006. Using circular dichroism spectra to estimate protein secondary structure. Nat. Protoc. 1, 2876–2890. https://doi.org/10.1038/nprot.2006.202.

Gurung, A.B., Ali, M.A., Lee, J., Farah, M.A., Al-Anazi, K.M., Sami, H., 2022. Molecular modelling studies unveil potential binding sites on human serum albumin for selected experimental and in silico COVID-19 drug candidate molecules. Saudi J. Biol. Sci. 29, 53–64. https://doi.org/10.1016/j.sjbs.2021.09.042.

Hanwell, M.D., Curtis, D.E., Lonie, D.C., Vandermeersch, T., Zurek, E., Hutchison, G.R., 2012. Avogadro: an advanced semantic chemical editor, visualization, and analysis platform. J. Cheminformat. 4 https://doi.org/10.1186/1758-2946-4-17.

Jiao, Y.H., Meng, F.Y., Zhu, G.B., Ran, L.Z., Jiang, Y.F., Zhang, Q., 2019. Synthesis of a novel p-hydroxycinnamic amide with anticancer capability and its interaction with human serum albumin. Exp. Ther. Med. 17, 1321–1329. https://doi.org/10.3892/etm.2018.7060.

Jorgensen, W.L., Chandrasekhar, J., Madura, J.D., Impey, R.W., Klein, M.L., 1983. Comparison of simple potential functions for simulating liquid water. J. Chem. Phys. 79, 926–935. https://doi.org/10.1063/1.445869.

Juarez, J., Taboada, P., Mosquera, V., 2009. Existence of different structural intermediates on the fibrillation pathway of human serum albumin. Biophys. J. 96, 2353–2370. https://doi.org/10.1016/j.bpj.2008.12.3901.

Lakowicz, J.R., 2006. Instrumentation for fluorescence spectroscopy. In: Lakowicz, J.R. (Ed.), Principles of Fluorescence Spectroscopy. Springer US, Boston, MA, pp. 27–61. https://doi.org/10.1007/978-0-387-46312-4_2.

Larkin, J., Ascierto, P.A., Dreno, B., Atkinson, V., Liszkay, G., Maio, M., Mandala, M., Demidov, L., Stroyakovskiy, D., Thomas, L., de la Cruz-Merino, L., Dutriaux, C., Garbe, C., Sovak, M.A., Chang, I., Choong, N., Hack, S.P., McArthur, G.A., Ribas, A., 2014. Combined vemurafenib and cobimetinib in BRAF-mutated melanoma. N. Engl. J. Med. 371, 1867–1876. https://doi.org/10.1056/NEJMoa1408868.

Leggio, C., Galantini, L., Pavel, N.V., 2008. About the albumin structure in solution: cigar Expanded form *versus* heart Normal shape. Phys. Chem. Chem. Phys. 10, 6741–6750. https://doi.org/10.1039/b808938h.

Matyus, L., Szollosi, J., Jenei, A., 2006. Steady-state fluorescence quenching applications for studying protein structure and dynamics. J. Photochem. Photobiol. B 83, 223–236. https://doi.org/10.1016/j.jphotobiol.2005.12.017.

Miller, R., Walker, S., Shui, I., Brandtmuller, A., Cadwell, K., Scherrer, E., 2020. Epidemiology and survival outcomes in stages II and III cutaneous melanoma: a systematic review. Melanoma Manag. 7, MMT39. https://doi.org/10.2217/mmt-2019-0022.

Mohseni-Shahri, F.S., Housaindokht, M.R., Bozorgmehr, M.R., Moosavi-Movahedi, A.A., 2016. Influence of taxifolin on the human serum albumin-propranolol interaction: multiple spectroscopic and chemometrics investigations and molecular dynamics simulation. J. Solution Chem. 45, 265–285. https://doi.org/10.3390/antiox12040815.

Pace, C.N., Vajdos, F., Fee, L., Grimsley, G., Gray, T., 1995. How to measure and predict the molar absorption coefficient of a protein. Protein Sci. 4, 2411–2423. https://doi.org/10.1002/pro.5560041120.

Pettersen, E.F., Goddard, T.D., Huang, C.C., Couch, G.S., Greenblatt, D.M., Meng, E.C., Ferrin, T.E., 2004. UCSF chimera - a visualization system for exploratory research and analysis. J. Comput. Chem. 25, 1605–1612. https://doi.org/10.1002/jcc.20084.

Pfizer, 2023. Pfizer Medical Information. BRAFTOVI®Clinical Pharmacology (encorafenib) | Pfizer Medical Information - US. https://www.pfizermedicalinformation.com/en-us/braftovi/clinical-pharmacology. Accessed 25 May 2023.

Rabbani, G., Ahmad, E., Khan, M.V., Ashraf, M.T., Bhat, R., Khan, R.H., 2015. Impact of structural stability of cold adapted Candida antarctica lipase B (CaLB): in relation to pH, chemical and thermal denaturation. RSC Adv. 5, 20115–20131. https://doi.org/10.1039/C4RA17093H.

Rabbani, G., Ahn, S.N., 2019. Structure, enzymatic activities, glycation and therapeutic potential of human serum albumin: a natural cargo. Int. J. Biol. Macromol. 123, 979–990. https://doi.org/10.1016/j.ijbiomac.2018.11.053.

Rabbani, G., Baig, M.H., Lee, E.J., Cho, W.K., Ma, J.Y., Choi, I., 2017. Biophysical study on the interaction between eperisone hydrochloride and human serum albumin using spectroscopic, calorimetric, and molecular docking analyses. Mol. Pharm. 14, 1656–1665. https://doi.org/10.1021/acs.molpharmaceut.6b01124.

Rabbani, G., Kaur, J., Ahmad, E., Khan, R.H., Jain, S.K., 2014. Structural characteristics of thermostable immunogenic outer membrane protein from Salmonella enterica serovar Typhi. Appl. Microbiol. Biotechnol. 98, 2533–2543. https://doi.org/10.1007/s00253-013-5123-3.

Rheault, T.R., Stellwagen, J.C., Adjabeng, G.M., Hornberger, K.R., Petrov, K.G., Waterson, A.G., Dickerson, S.H., Mook Jr., R.A., Laquerre, S.G., King, A.J., Rossanese, O.W., Arnone, M.R., Smitheman, K.N., Kane-Carson, L.S., Han, C., Moorthy, G.S., Moss, K.G., Uehling, D.E., 2013. Discovery of dabrafenib: a selective inhibitor of Raf Kinases with antitumor activity against B-Raf-Driven tumors. ACS Med. Chem. Lett. 4, 358–362. https://doi.org/10.1021/ml4000063.

Roberts, J.A., Pea, F., Lipman, J., 2013. The clinical relevance of plasma protein binding changes. Clin. Pharmacokinet. 52, 1–8. https://doi.org/10.1007/s40262-012-0018-5.

Roe, D.R., Cheatham 3rd, T.E., 2013. PTRAJ and CPPTRAJ: software for processing and analysis of molecular dynamics trajectory data. J. Chem. Theory Comput. 9, 3084–3095. https://doi.org/10.1021/ct400341p.

Ross, P.D., Subramanian, S., 1981. Thermodynamics of protein association reactions: forces contributing to stability. Biochemistry 20, 3096–3102. https://doi.org/10.1021/bi00514a017.

Russi, M., Cavalieri, G., Marson, D., Laurini, E., Pricl, S., 2022. Binding of the B-raf inhibitors dabrafenib and vemurafenib to human serum albumin: a biophysical and molecular simulation study. Mol. Pharm. 19, 1619–1634. https://doi.org/10.1021/acs.molpharmaceut.2c00100.

Saboury, A.A., 2006. A review on the ligand binding studies by isothermal titration calorimetry. J. Iran. Chem. Soc. 3, 1–21. https://doi.org/10.1007/BF03245784.

Saginala, K., Barsouk, A., Aluru, J.S., Rawla, P., Barsouk, A., 2021. Epidemiology of melanoma. Med. Sci. (Basel) 9. https://doi.org/10.3390/medsci9040063.

Santos, A.S., Mora-Ocampo, I.Y., de Novais, D.P.S., Aguiar, E., Pirovani, C.P., 2023. State of the art of the molecular biology of the interaction between cocoa and witches' broom disease: a systematic review. Int. J. Mol. Sci. 24 https://doi.org/10.3390/ijms24065684.

SEER, 2023. Surveillance, epidemiology, and end results; 'Melanoma of the Skin - Cancer Stat Facts'. https://seer.cancer.gov/statfacts/html/melan.html. Accessed 15 June 2023.

Shirley, M., 2018. Encorafenib and binimetinib: first global approvals. Drugs 78, 1277–1284. https://doi.org/10.1007/s40265-018-0963-x.

Sridharan, R., Zuber, J., Connelly, S.M., Mathew, E., Dumont, M.E., 2014. Fluorescent approaches for understanding interactions of ligands with G protein coupled receptors. Biochim. Biophys. Acta 1838, 15–33. https://doi.org/10.1016/j.bbamem.2013.09.005.

Su, H., Xu, Y., 2018. Application of ITC-based characterization of thermodynamic and kinetic association of ligands with proteins in drug design. Front. Pharmacol. 9, 1133. https://doi.org/10.3389/fphar.2018.01133.

Sudlow, G., Birkett, D.J., Wade, D.N., 1975. Spectroscopic techniques in the study of protein binding. A fluorescence technique for the evaluation of the albumin binding and displacement of warfarin and warfarin-alcohol. Clin. Exp. Pharmacol. Physiol. 2, 129–140. https://doi.org/10.1111/j.1440-1681.1975.tb01826.x.

Tang, B., Tang, P., He, J., Yang, H., Li, H., 2018. Characterization of the binding of a novel antitumor drug ibrutinib with human serum albumin: insights from spectroscopic, calorimetric and docking studies. J. Photochem. Photobiol. B 184, 18–26. https://doi.org/10.1016/j.jphotobiol.2018.05.008.

Tayeh, N., Rungassamy, T., Albani, J.R., 2009. Fluorescence spectral resolution of tryptophan residues in bovine and human serum albumins. J. Pharm. Biomed. Anal. 50, 107–116. https://doi.org/10.1016/j.jpba.2009.03.015.

Teixido, C., Castillo, P., Martinez-Vila, C., Arance, A., Alos, L., 2021. Molecular markers and targets in melanoma. Cells 10. https://doi.org/10.3390/cells10092320.

Trott, O., Olson, A.J., 2010. Software news and update AutoDock Vina: improving the speed and accuracy of docking with a new scoring function, efficient optimization, and multithreading. J. Comput. Chem. 31, 455–461. https://doi.org/10.1002/jcc.21334.

van de Weert, M., Stella, L., 2011. Fluorescence quenching and ligand binding: a critical discussion of a popular methodology. J. Mol. Struct. 998, 144–150. https://doi.org/10.1016/j.molstruc.2011.05.023.

Wang, L., Wu, X., Yang, Y., Liu, X., Zhu, M., Fan, S., Wang, Z., Xue, J., Hua, R., Wang, Y., Li, Q.X., 2019a. Multi-spectroscopic measurements, molecular modeling and density functional theory calculations for interactions of 2,7-dibromocarbazole and 3,6-dibromocarbazole with serum albumin. Sci. Total Environ. 686, 1039–1048. https://doi.org/10.1016/j.scitotenv.2019.06.001.

Wang, Y., Wang, L.J., Zhu, M.Q., Xue, J.Y., Hua, R.M., Li, Q.X., 2019b. Comparative studies on biophysical interactions between gambogic acid and serum albumin via multispectroscopic approaches and molecular docking. J. Lumin. 205, 210–218. https://doi.org/10.1016/j.jlumin.2018.09.005.

Wang, Y., Yu, H.Y., Shi, X.L., Luo, Z.P., Lin, D.H., Huang, M.D., 2013. Structural mechanism of ring-opening reaction of glucose by human serum albumin. J. Biol. Chem. 288, 15980–15987. https://doi.org/10.1074/jbc.M113.467027.

Zargar, S., Wani, T.A., Alsaif, N.A., Khayyat, A.I.A., 2022. A comprehensive investigation of interactions between antipsychotic drug quetiapine and human serum albumin using multi-spectroscopic, biochemical, and molecular modeling approaches. Molecules 27. https://doi.org/10.3390/molecules27082589.

Zhao, Z., Shi, T., Chu, Y., Cao, Y., Cheng, S., Na, R., Wang, Y., 2022. Comparison of the interactions of flupyrimin and nitenpyram with serum albumins via multiple analysis methods. Chemosphere 289, 133139. https://doi.org/10.1016/j.chemosphere.2021.133139.

Zhivkova, Z.D., 2015. Studies on drug-human serum albumin binding: the current state of the matter. Curr. Pharm. Des. 21, 1817–1830. https://doi.org/10.2174/1381612821666150302113710.

Zsila, F., 2013. Subdomain IB is the third major drug binding region of human serum albumin: toward the three-sites model. Mol. Pharm. 10, 1668–1682. https://doi.org/10.1021/mp400027q.